Canopy height and climate dryness parsimoniously explain spatial variation of unstressed stomatal conductance

Yanlan Liu[1], Olivia Flournoy[2], Quan Zhang[3], Kimberly Novick[4], Randal D. Koster[5], and Alexandra Konings[2]

[1]The Ohio State University
[2]Stanford University
[3]Wuhan University
[4]Indiana University Bloomington
[5]NASA Goddard SFC

November 24, 2022

Abstract

The spatio-temporal variation of stomatal conductance directly regulates photosynthesis, water partitioning, and biosphere-atmosphere interactions. While many studies have focused on stomatal response to stresses, the spatial variation of unstressed stomatal conductance remains poorly determined, and is usually characterized in land surface models (LSMs) simply based on plant functional type (PFT). Here, we derived unstressed stomatal conductance at the ecosystem-scale using observations from 115 global FLUXNET sites. When aggregated by PFTs, the across-PFT pattern was highly consistent with the parameterizations of LSMs. However, PFTs alone captured only 17\% of the variation in unstressed stomatal conductance across sites. Within the same PFT, unstressed stomatal conductance was negatively related to climate dryness and canopy height, which explained 45\% of the total spatial variation. Our results highlight the importance of plant-environment interactions in shaping stomatal traits. The trait-environment relationship established here provides an empirical approach for improved parameterizations of stomatal conductance in LSMs.

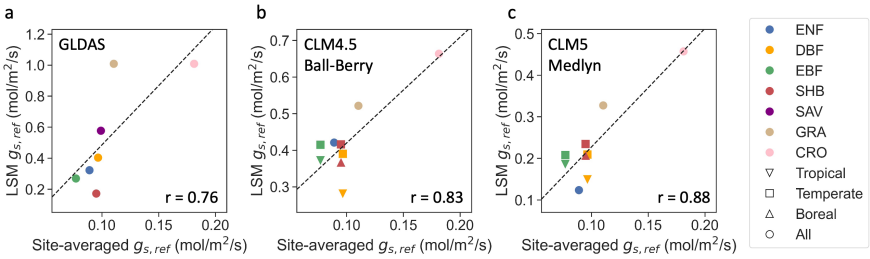

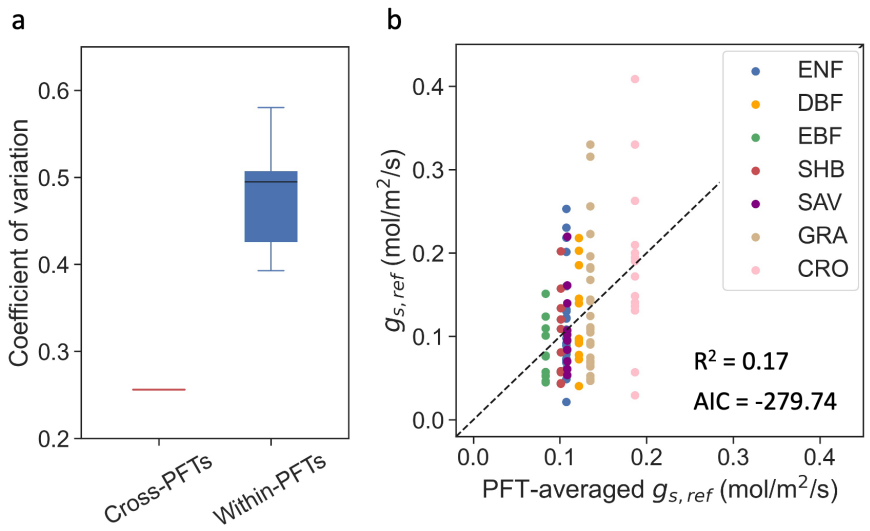

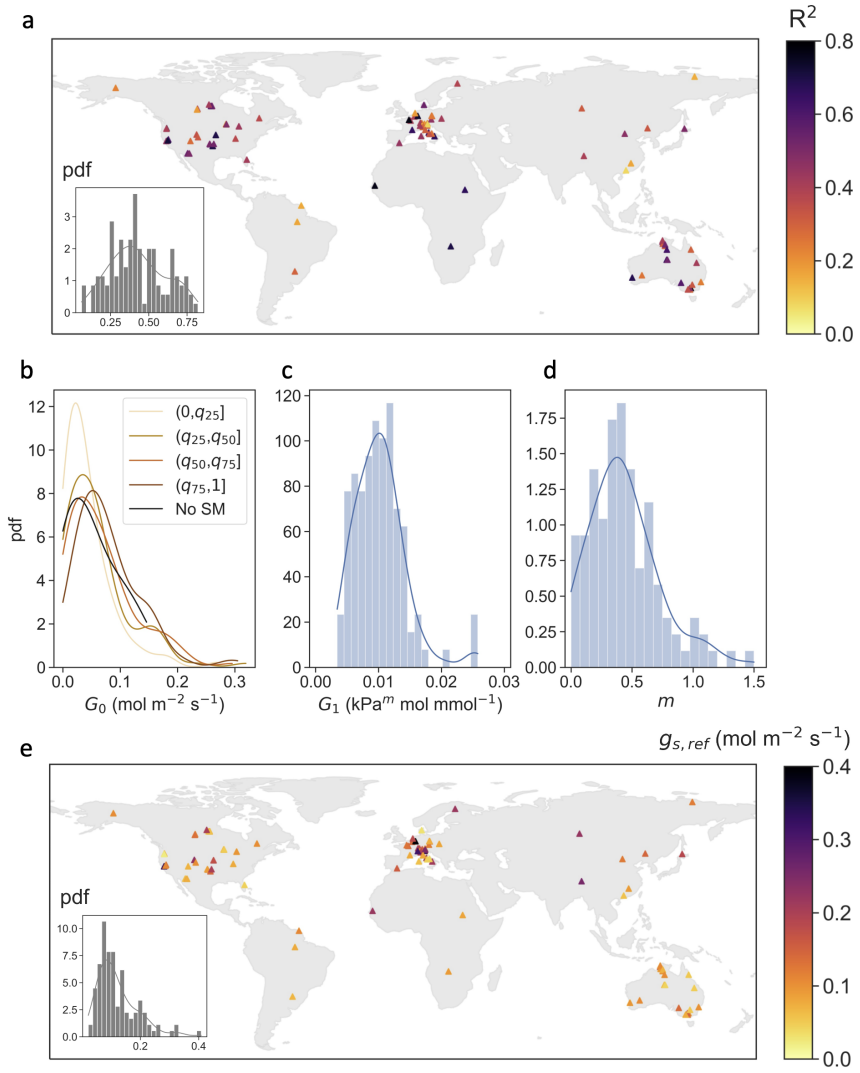

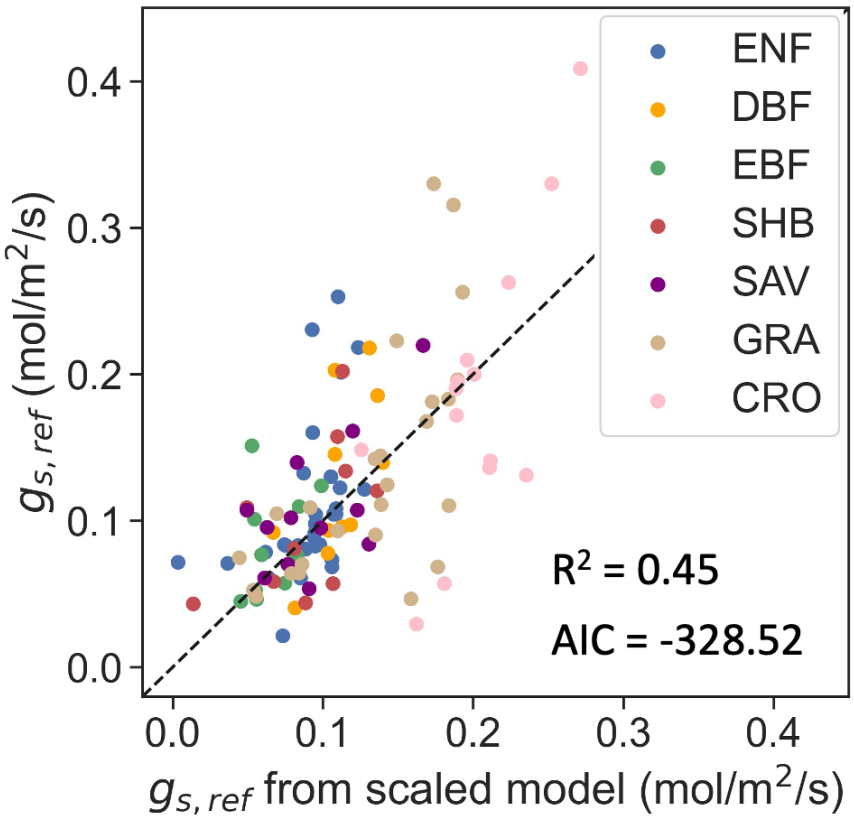

Canopy height and climate dryness parsimoniously explain spatial variation of unstressed stomatal conductance

Yanlan Liu [1,2], Olivia Flournoy [3], Quan Zhang [4], Kimberly A. Novick [5], Randal D. Koster [6], Alexandra G. Konings [7]

[1]School of Earth Sciences, The Ohio State University, Columbus, OH, USA
[2]School of Environment and Natural Resources, The Ohio State University, Columbus, OH, USA
[3]Department of Geophysics, Stanford University, Stanford, CA, USA
[4]State Key Laboratory of Water Resources and Hydropower Engineering Science, Wuhan University, Wuhan, China
[5]O'Neill School of Public and Environmental Affairs, Indiana University Bloomington, Bloomington, IN, USA
[6]Global Modeling and Assimilation Office, NASA GSFC, Greenbelt, MD, USA
[7]Department of Earth System Science, Stanford University, Stanford, CA, USA

Key Points:

- Many large-scale models represent the spatial patterns of unstressed stomatal conductance using plant functional types (PFTs)
- PFT-averages of unstressed stomatal conductance at FLUXNET sites only capture seventeen percent of spatial variability
- Spatial variation of unstressed stomatal conductance is better explained using climate dryness and canopy height

Corresponding author: Yanlan Liu, `liu.9367@osu.edu`

Abstract

The spatio-temporal variation of stomatal conductance directly regulates photosynthesis, water partitioning, and biosphere-atmosphere interactions. While many studies have focused on stomatal response to stresses, the spatial variation of unstressed stomatal conductance remains poorly determined, and is usually characterized in land surface models (LSMs) simply based on plant functional type (PFT). Here, we derived unstressed stomatal conductance at the ecosystem-scale using observations from 115 global FLUXNET sites. When aggregated by PFTs, the across-PFT pattern was highly consistent with the parameterizations of LSMs. However, PFTs alone captured only 17% of the variation in unstressed stomatal conductance across sites. Within the same PFT, unstressed stomatal conductance was negatively related to climate dryness and canopy height, which explained 45% of the total spatial variation. Our results highlight the importance of plant-environment interactions in shaping stomatal traits. The trait-environment relationship established here provides an empirical approach for improved parameterizations of stomatal conductance in LSMs.

Plain Language Summary

Stomatal conductance regulates the ease with which vegetation extracts water from the soil and releases it to the atmosphere. It thus helps determine the total evapotranspiration and plant uptake of carbon, which in turn significantly influences many aspects of ecosystem function, ranging from regional water resources to biodiversity and climate feedbacks. In particular, stomatal conductance under a stress-free condition (without limitations from water, light, or other factors) acts as the basis of all mathematical models of stomatal dynamics. It is important to understand what causes the unstressed conductance to vary from one place to the next. Large-scale models often assume the unstressed stomatal conductance is the same for all ecosystems belonging to the same plant functional type (for example, deciduous forests, grasslands, or croplands). However, based on observations at 115 sites across the globe, we showed that unstressed stomatal conductance varies significantly between sites within the same plant functional type. Sites located in drier climates and with taller canopies tended to have lower unstressed stomatal conductance. Accounting for climate dryness and canopy height helped better explain the spatial variation. Our results provide a useful approach to improving model descriptions of stomatal conductance.

1 Introduction

Stomatal conductance for water vapor and carbon dioxide is a primary control on transpiration and photosynthesis. Many aspects of ecosystem function, including water resources (Fowler et al., 2019; Mankin et al., 2019), carbon sink strength (Powell et al., 2013; Trugman et al., 2018), tree mortality (McDowell et al., 2011; Anderegg et al., 2018), regional climate feedbacks (Kala et al., 2016; Green et al., 2017), and ecoclimate telecommunications (Garcia et al., 2016; Stark et al., 2016), are directly regulated by the spatio-temporal variation of stomatal conductance. Representation of this variation has been recognized as the central link of biosphere-atmosphere interactions in observational and modeling studies (Hetherington & Woodward, 2003; Buckley & Mott, 2013; Bonan et al., 2014; Franks et al., 2018). Under reference conditions of low water stress and non-limiting radiation and temperature, the open apertures of stomata lead to unstressed stomatal conductance ($g_{s,\mathrm{ref}}$). During periods of water, light, or temperature stress, stomata close, thus downregulating stomatal conductance. Over the past decades, much attention has been focused on evaluating the reduction of stomatal conductance in response to meteorological conditions and water stress (Powell et al., 2013; Novick et al., 2016; Sperry et al., 2017; Konings et al., 2017; Trugman et al., 2018; Y. Liu et al., 2020). However, although $g_{s,\mathrm{ref}}$ is the reference basis for downregulation of stomatal conductance under all meteorological conditions, its spatial variation remains poorly understood. Due to the direct influence of $g_{s,\mathrm{ref}}$ on biosphere-atmosphere interactions during both stressed and non-stressed conditions, an accurate description of the spatial variation of $g_{s,\mathrm{ref}}$ is fundamental for predictions of ecosystem dynamics in space and time.

In-situ measurements have found a negative relationship between $g_{s,\mathrm{ref}}$ and canopy height at the tree scale (Ryan et al., 2000; Schäfer et al., 2000; Novick et al., 2009), supporting the hydraulic limitation hypothesis (Ryan et al., 2006). This theory predicts that, under steady-state flow conditions, the $g_{s,\mathrm{ref}}$ should be coordinated with xylem conductance, which itself is inversely related to the soil-to-leaf path length, i.e., canopy height. Nonetheless, observations suggesting a positive relationship between $g_{s,\mathrm{ref}}$ and canopy height also exist (McDowell et al., 2002). This may be because taller canopies have greater sapwood area per leaf area, thus contributing to a higher xylem conductance and thus greater $g_{s,\mathrm{ref}}$ (Fischer et al., 2002). The overall balance of these two factors remains unclear. Moreover, leaf-scale measurements have found that species in more arid climates tend to have lower stomatal density and area (Carlson et al., 2016; C. Liu et al., 2018).

Because $g_{s,\mathrm{ref}}$ is morphologically determined at the leaf scale by these factors (Franks et al., 2009; Lammertsma et al., 2011; Dow et al., 2014), these measurements suggest a negative relationship between $g_{s,\mathrm{ref}}$ and climate dryness. However, the observational studies were based on measurements at leaf and tree scales with a limited number of species. It remains unclear whether these relationships explaining the spatial variation of $g_{s,\mathrm{ref}}$ are generalizable to the ecosystem-scale. Furthermore, each of the observational studies tested an independent correlation between $g_{s,\mathrm{ref}}$ and an individual covariate. The combined effect requires further investigation.

Addressing this gap is particularly relevant for land surface models (LSMs), which typically omit spatial variation of $g_{s,\mathrm{ref}}$ other than that due to the distribution of plant functional types (PFTs). Specifically, $g_{s,\mathrm{ref}}$ in LSMs corresponds to the stomatal conductance under optimal meteorological conditions and no soil moisture limitation, represented using empirical or optimal approaches, e.g., the Jarvis, Ball-Berry and Medlyn models (Jarvis, 1976; Ball et al., 1987; Medlyn et al., 2011; Franks et al., 2018). The spatial pattern of $g_{s,\mathrm{ref}}$ is determined by a single parameter or an equivalent parameter set (e.g., the slope parameter, the maximum photosynthetic carboxylation rate $V_{c,\max}$, etc.) assigned for each PFT. However, previous studies have found many related plant traits, such as $V_{c,\max}$ and multiple hydraulic traits, vary significantly within a PFT (Anderegg, 2015; Walker et al., 2017; Konings & Gentine, 2017; Y. Liu et al., 2021), which can incur large errors in stomatal closure modeling (Wolz et al., 2017). These variations can, among others, emerge from plant-environment interactions and community dynamics, through which the environment can be considered as a filter in shaping the community-average traits (Cornwell et al., 2006; Ackerly & Cornwell, 2007). Such "environmental filtering" has previously been applied in large-scale models to improve the parameterization of photosynthetic traits and empirical evapotranspiration parameters by mapping them to climate and environmental characteristics (Verheijen et al., 2015; Walker et al., 2017; Wu et al., 2020). In the same way, $g_{s,\mathrm{ref}}$ may also vary with ecological and environmental conditions as a result of plant-environment interactions.

Our objective is to explore the extent to which information about canopy height and climate dryness predict spatial variation in ecosystem scale $g_{s,\mathrm{ref}}$. We use observations at 115 FLUXNET sites to derive $g_{s,\mathrm{ref}}$ and hypothesize that $g_{s,\mathrm{ref}}$ varies with canopy height and climatic factors, including mean annual air temperature, mean annual precipitation, and climate dryness across sites. We examine whether an environmental fil-

ter exists that could characterize the spatial variation of $g_{s,\mathrm{ref}}$ better than the PFT-based approach widely used in LSMs. Our analysis aims to parsimoniously explain the spatial variation of $g_{s,\mathrm{ref}}$ within PFTs using readily available datasets, thus providing a tractable approach to better parameterize stomatal conductance in LSMs.

2 Methods

2.1 Sites and datasets

The 115 global FLUXNET sites covered seven PFTs and a wide range of climates. Among the sites included in the FLUXNET2015 Tier1 dataset (FLUXNET, 2016), we analyzed only those with ET and relevant meteorological data available, and for which there were at least 100 valid observations satisfying the quality control filters described in Section 2.2. The PFT of each site is determined based on the International Geosphere-Biosphere Programme (IGBP) classification system. The sites include 31 evergreen needle-leaf forests, 12 deciduous broadleaf forests, 11 evergreen broadleaf forests, 10 shrublands, 12 savannas, 25 grasslands, and 14 croplands. Leaf area index was extracted from the closest 500 m pixel from the MODIS (Moderate Resolution Imaging Spectroradiometer) product (MCD15A3H.006) using Google Earth Engine (Myneni et al., 2015) with a 4-day temporal resolution. It was then smoothed using the Savitzky–Golay filter to remove high-frequency noise and linearly interpolated to the same temporal resolution (half-hourly or hourly, depending on the site) as the flux measurements. Canopy height was obtained from the Biological, Ancillary, Disturbance and Metadata (BADM) associated with the FLUXNET2015 dataset.

2.2 Derivation of unstressed stomatal conductance

Ecosystem conductance (G_s) was calculated by inverting the Penman-Monteith equation (Penman, 1948; Monteith, 1965) using ET and relevant meteorological conditions at a half-hourly or hourly scale, including net radiation, air temperature, relative humidity, wind speed, and friction velocity. To control the uncertainty in the estimated conductance, only measurements taken between 10 am and 3 pm that satisfy the following filters were used: no rainfall in the previous two days, net radiation greater than half of the annual maximum, vapor pressure deficit greater than 0.6 kPa, and wind speed greater than 1 m/s. More details on the inversion method are described in Zhang et al. (2019).

We note that G_s estimated by inverting the Penman-Monteith equation is subject to bias, which remains challenging to accurately quantify due to biased or unmeasured energy budget components (Wehr & Saleska, 2021). While this bias has been shown to cause skewed down-regulation sensitivities of stomatal conductance to light and moisture stresses (Wehr & Saleska, 2021), we only analyze stomatal conductance under close-to-optimal conditions at all sites here. Notably, for sites with available observations of energy budget components, we tested only using the data when the energy closure error is below average and found the main results remained fundamentally unchanged (Fig. S1). Thus, this uncertainly will likely contribute to unexplained residuals but not qualitatively change the derived relationships.

The ecosystem conductance was then partitioned into soil conductance and canopy conductance using a data-driven approach that generalizes Leuning's and Medlyn's models of stomatal conductance (C. Lin et al., 2018; X. Li et al., 2019):

$$G_s = G_0 + G_1 \frac{\mathrm{GPP}}{\mathrm{VPD}^m} \tag{1}$$

where GPP is the gross primary production; VPD is the vapor pressure deficit; and G_0, G_1, and m are parameters fitted by minimizing the root-mean-square error. As discussed in more detail below, we assume that, at the ecosystem scale, G_0 is dominated by soil conductance. One set of fitting parameters was estimated for each site using all available data from the growing season, which was identified based on LAI being greater than its median. Because G_0 can vary with soil moisture, the parameters were fitted using data binned by the quartiles of soil moisture measurements at each site for which soil moisture measurements were available, and using all valid data otherwise (at 16 sites). The accuracy of Eq. 1 was evaluated at each site. We subtracted the fitted constants G_0 at different soil moisture levels from the hourly/half-hourly ecosystem conductance G_s to approximate canopy conductance, which preserves the original variation of G_s and reduces the uncertainty introduced by fitting errors.

The canopy conductance was then scaled to stomatal conductance (g_s) at leaf-scale using LAI as follows.

$$g_s = \frac{(G_s - G_0)}{\min(\mathrm{LAI}, 6)} \tag{2}$$

The cut-off point of LAI = 6 was used to account for the nonlinear scaling between stomata and canopy conductances due to shading in dense canopy (Granier et al., 2000; Novick et al., 2009; Alam et al., 2021). Lastly, the unstressed stomatal conductance ($g_{s,\mathrm{ref}}$) was

quantified as the 90th percentile of the g_s time series satisfying all the filters described above at each site. The 90th percentile was used to approximate the maximum stomatal conductance while minimizing the impact of outliers due to observational noise. We note that because the optimal temperature, saturated radiation, and minimal water stress rarely co-occur, $g_{s,\mathrm{ref}}$ is expected to be lower than but correlated to the maximum stomatal conductance, as also found in leaf-scale measurements (Dow et al., 2014; McElwain et al., 2016). Thus, through this work, the term "unstressed conductance" may not represent the truly maximum conductance, but rather the conductance observed under environmental conditions that are reasonably close to optimal.

We adopted several approaches to evaluate the uncertainties inherent to our approach. First, we tested the robustness of our method to errors in the separation of soil and canopy conductance, such as in the case where there is an intercept in the stomatal conductance-GPP relationship due to cuticular conductance, incompletely closed stomata, or other reasons (Medlyn et al., 2011; Duursma et al., 2019). In this case, G_0 also represents part of the canopy conductance. In the extreme case (i.e., no soil conductance contribution to G_0), instead of Eq. 2, g_s could be calculated as $g_s = G_s/\min(\mathrm{LAI}, 6)$. Combined with g_s derived from Eq. 2, these two estimates span the possible range of zero to large contributions of stomatal conductance to G_0, allowing us to test the robustness of our results to G_s partitioning uncertainty. Second, we tested different thresholds for the cut-off point (LAI = 4, 6, and 8) used to scale the canopy conductance to stomatal conductance. Finally, while $g_{s,\mathrm{ref}}$ represents stomatal conductance under close-to-optimal conditions at all sites, the hydroclimatic conditions when $g_{s,\mathrm{ref}}$ was achieved could be farther away from the optima at some sites than others. For example, in most sites, g_s close to $g_{s,\mathrm{ref}}$ was found around VPD of 1 kPa, as expected theoretically (Oren et al., 1999); however, in extremely dry sites, it was only found when VPD exceeded 1.5 kPa (Fig. S2). To better understand whether this difference is attributable to real variations or to the methodological choice to surrogate $g_{s,\mathrm{ref}}$ to the 90th percentile of $g_{s,\mathrm{ref}}$, we calculated an alternative $g_{s,\mathrm{ref}}$ as the envelope (90th quantile) of g_s under VPD = 1 kPa using a quantile regression (Fig. S3) (Koenker, 2005).

2.3 Baseline model and scaled model estimating $g_{s,\mathrm{ref}}$ variation

Two models for estimating spatial variation of $g_{s,\mathrm{ref}}$ were compared: a 'baseline model' that is an analogy of the PFT-based approach used in land models and a 'scaled model'

that parsimoniously accounts for relations with canopy height and climate conditions, i.e., environmental filters. The baseline model was derived by calculating the average of $g_{s,\mathrm{ref}}$ for all FLUXNET sites, and can be written as:

$$y_i^j = c^j + \delta_i \tag{3}$$

where y_i^j is the $g_{s,\mathrm{ref}}$ at the ith site belonging to the jth PFT; c^j is the jth PFT-specific parameter, equal to the average $g_{s,\mathrm{ref}}$ of the jth PFT; and δ_i is the model error.

To test whether an environmental filter could better estimate $g_{s,\mathrm{ref}}$ variation, a scaled model was used, which describes $g_{s,\mathrm{ref}}$ as a fixed linear combination of explanatory variables that is multiplicatively scaled by a PFT-specific factor.

$$y_i^j = \alpha^j(\beta^T X_i) + \delta_i \tag{4}$$

where X_i is a vector containing z-scores of a set of explanatory variables for the ith site, and β contains the corresponding coefficients. Z-scores rather than the original magnitudes of explanatory variables were used in X_i so that β^T reflects the relative sensitivities. Note that the vector β^T is independent of PFT j, maintaining the same ratio of sensitivity to each of the possible explanatory variables X_i. By maintaining this consistency, the number of necessary variables is reduced significantly, preserving the parsimonious nature of the model and preventing over-fitting. The PFT-specific parameter α^j accounts for different scalings across PFTs. For X_i, we explored widely-available variables (to ensure a large dataset and tractability of the resulting model as an environmetal filter) of three categories: long-term average precipitation and air temperature, dryness index, and canopy height (Table 1). Mean annual air temperature (MAT) and precipitation (MAP) were calculated using the FLUXNET2015 dataset as averages across the entire record of each site. We considered six different metrics to quantify climate dryness based on actual evapotranspiration (ET), potential evapotranspiration (PET) and MAP. PET was calculated using the Penman-Monteith equation, and ET was calculated as the average of the observations across the entire record period. The inverse of canopy height ($1/H_c$), rather than canopy height itself, was used because the inverse linearly controls the xylem conductance from the root to the leaf, which affects stomatal conductance through hydraulic coordination (Brodribb & Jordan, 2011; Manzoni et al., 2013). To identify the most informative variables, we conducted model selection by choosing at most one variable within each of the three categories. The performance of models with different variable combinations was evaluated using the coefficient of determination (R^2)

and the Akaike information criteria (AIC). We analyzed the top ten scaled models (based on AIC) and compared their AIC and R^2 to the baseline model. We further examined the relation between $g_{s,\mathrm{ref}}$ and the selected independent variables as reflected by β. The uncertainty of β of the best-performing model was estimated using seven-fold bootstrapping (Efron, 1992).

Table 1. Candidate variables considered in the scaled model

	Candidate variables					
Canopy height	$1/H_c$					
Dryness index	PET/MAP	PET–MAP	PET/ET	PET–ET	ET/MAP	ET–MAP
Mean climate	MAP	MAT				

2.4 Unstressed stomatal conductance within land surface models

We compared the baseline model derived here from FLUXNET sites to the actual parameterizations used in land surface models and a global modeling system. The Global Land Data Assimilation System (GLDAS) (Rodell et al., 2004), the Community Land Model Version 4.5 (CLM4.5) (Oleson et al., 2013) and Version 5 (CLM5) (Lawrence et al., 2019) were used as examples. The land model Noah v3.3 in GLDAS prescribes unstressed stomatal conductance per PFT, and these values were directly compared with $g_{s,\mathrm{ref}}$ here. CLM4.5 and CLM5 describe stomatal conductance using the Ball-Berry model and the Medlyn model respectively; in these two models, the unstressed stomatal conductance is not directly prescribed but primarily determined by the maximum rate of Rubisco carboxylase activity V_{cmax} and the slope parameter g_1, which are specified by PFT. We calculated the equivalent unstressed stomatal conductance of each PFT using the PFT-specific parameters as in Oleson et al. (2013) and Lawrence et al. (2019) under reference conditions, i.e., net radiation of 600 W/m^2, air and leaf temperature of 25 °C, VPD of 0.6 kPa, and without soil moisture limitation. The maximum rate of photosynthetic electron transport (J_{max}) and the photorespiration rate were approximated as 1.97 and 0.015 times $V_{c,max}$, respectively (Oleson et al., 2013).

3 Results and Discussion

3.1 Unstressed stomatal conductance across sites

Across sites, the ecosystem conductance model (Eq. 1) captures on average 43% and up to 82% of subdaily variation of the derived ecosystem conductance G_s (Fig. 1a). This is on par with an R^2 of 0.52 at one site reported in C. Lin et al. (2018). The model R^2 does not exhibit clear spatial clusters (Fig. 1a) and does not significantly differ for sites with and without soil moisture measurements ($p > 0.1$ using a Kolmogorov–Smirnov test). At sites with available soil moisture measurements, G_0 increases with soil moisture as expected. The across-sites medians of G_0 are 0.043, 0.059, 0.066, and 0.080 mol/m^2/s under soil moisture within the first to the fourth quartiles, respectively (Fig. 1b). The mid-50% of the slope (G_1) and the exponent (m) parameters range from 0.075 to 0.121 (kPa^m mol μmol^{-1}), and from 0.240 to 0.584, respectively (Fig. 1c, d). The values of all three parameters estimated here are consistent with those in previous studies (C. Lin et al., 2018; X. Li et al., 2019).

The derived $g_{s,\mathrm{ref}}$ spans a wide range from 0.022 to 0.409 mol/m^2/s (Fig. 1e) and is not clustered by PFT or climate type. Each of the tropical, temperate and boreal regions and all of the PFTs include both small (below the 25th percentile across all sites) and large (above the 75th percentile) values of $g_{s,\mathrm{ref}}$. The large spatial variability of $g_{s,\mathrm{ref}}$ highlights the need for its appropriate characterization.

3.2 Cross-PFT pattern and connection to parameterization of LSMs

The PFT-averaged $g_{s,\mathrm{ref}}$ is highest in croplands (0.186 mol/m^2/s), followed by grasslands (0.135 mol/m^2/s), and is lowest in evergreen broadleaf forests (0.083 mol/m^2/s). This cross-PFT pattern is largely consistent with the parameterization of LSMs (Fig. 2). The equivalent $g_{s,\mathrm{ref}}$ from GLDAS, CLM4.5 and CLM5 are correlated with the site-averaged $g_{s,\mathrm{ref}}$ per PFT with Pearson correlation coefficients of 0.76, 0.83, and 0.88 respectively ($p < 0.01$ for all), though these correspondences are in large part attributable to high $g_{s,\mathrm{ref}}$ in croplands. When excluding croplands, the correlations degrade to 0.78, 0.55, and 0.31 for the three model parameterizations, respectively. While the cross-PFT patterns derived here and the parametrization of LSMs are largely consistent, significant differences also remain. These may be attributable to the limited number of sites in each

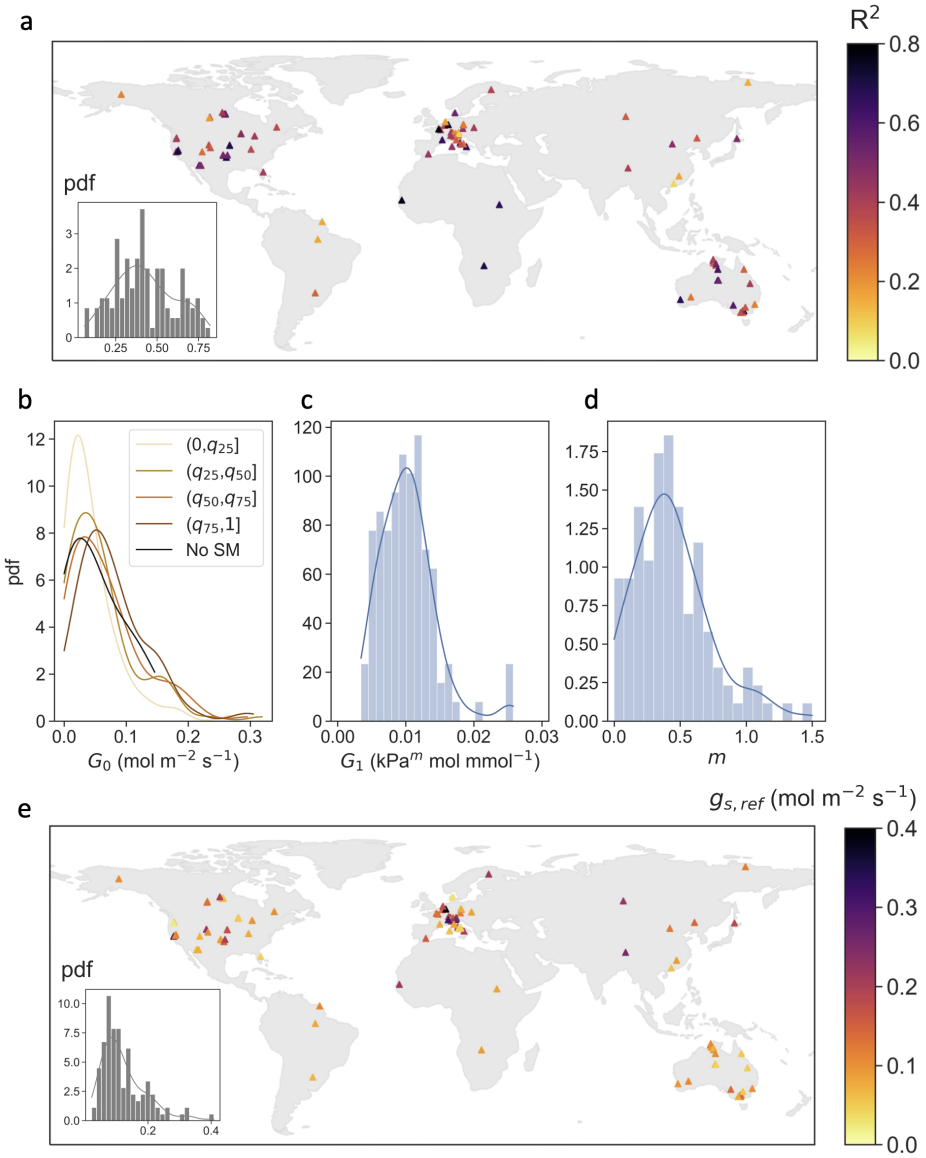

Figure 1. (a) Temporal variation of ecosystem conductance G_s explained by the ecosystem conductance model (Eq. 1) for all investigated FLUXNET sites. Model accuracy was evaluated using the coefficient of determination (R^2) between fitted G_s and that derived from observations. (b) Probability density function (pdf) of the fitted soil conductance (G_0) across sites under measured soil moisture in the four quartiles separated by the 25th (q_{25}), the 50th (q_{50}), and the 75th (q_{75}) quantiles of each site, and under all soil moisture conditions at sites without soil moisture measurement (no SM). (c) The pdf of the slope parameter G_1. (d) The pdf of the VPD-sensitivity parameter m. (e) The unstressed stomatal conductance ($g_{s,\mathrm{ref}}$) derived for FLUXNET sites.

PFT in this study and similarly, the small number of (possibly different) sites typically used to tune parameters in LSMs.

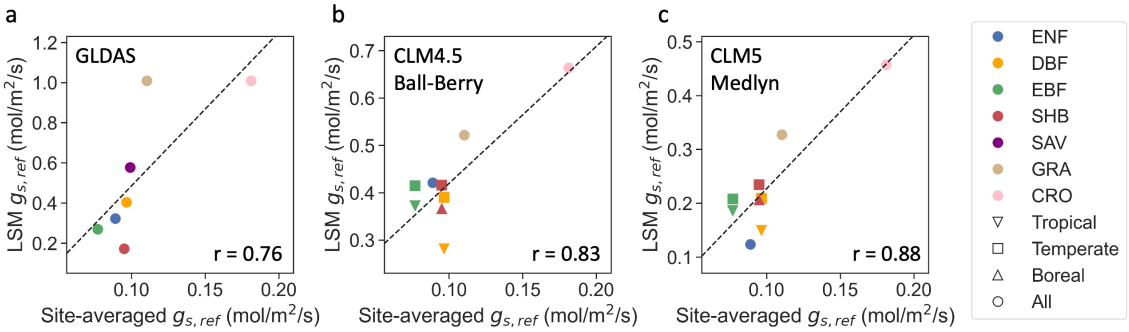

Figure 2. Relations between PFT-averaged unstressed stomatal conductance ($g_{s,\mathrm{ref}}$) of FLUXNET sites and the equivalent $g_{s,\mathrm{ref}}$ calculated using the parameterizations of (a) Noah v3.3 in GLDAS, (b) the Ball-Berry model in CLM4.5, and (c) the Medlyn model in CLM5. Black dashed lines denote the regression lines. Colored dots represent the seven PFTs, including evergreen needleleaf forests (ENF), deciduous broadleaf forests (DBF), evergreen broadleaf forests (EBF), shrublands (SHB, including both open and closed shrublands), savannas (SAV, including both savannas and woody savannas), grasslands (GRA), and croplands (CRO). Different symbol shapes denote parameterizations specific for tropical, temperate and boreal biomes. Each panel only shows available PFTs and biomes in the corresponding model.

On average, the cross-PFT variation of observed $g_{s,\mathrm{ref}}$ is only half of that seen within each of the seven PFTs (Fig. 3a). As a result, the PFT-averages of $g_{s,\mathrm{ref}}$ only explain 17% of the total observed variation across all sites (Fig. 3b). This suggests that representing the unstressed stomatal conductance via PFT alone ignores significant sources of spatial variation, which may result in spatial errors of simulated biosphere-atmosphere interactions in LSMs.

3.3 Improved spatial estimation of unstressed stomatal conductance

The most informative variable in explaining the spatial variation of $g_{s,\mathrm{ref}}$ is the dryness index, calculated as the long-term averaged deficit between potential evapotranspiration and the actual evapotranspiration (PET–ET), followed by canopy height. Using these two variables, the scaled model (Eq. 4) explains 45% of the variation of $g_{s,\mathrm{ref}}$ across all sites (Fig. 4), which more than doubles the R^2 of 0.17 using PFT-averages (Fig. 3).

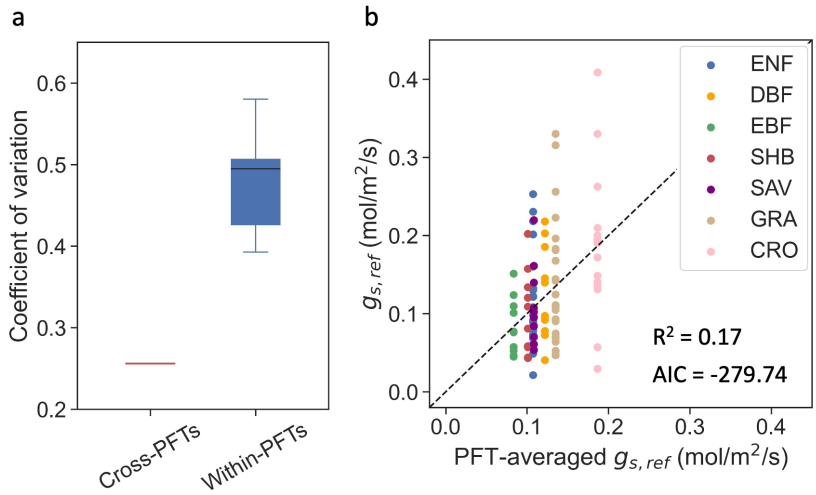

Figure 3. (a) The coefficient of variation of $g_{s,\mathrm{ref}}$ across- and within-PFTs. (b) Relation between PFT-averaged $g_{s,\mathrm{ref}}$ (the baseline model) and the $g_{s,\mathrm{ref}}$ across sites. Acronyms of PFTs are noted in the caption of Fig. 2.

Despite requiring more parameters, the best scaled model is also more informative (AIC= -328.52) than the baseline model (AIC= -279.74). The $g_{s,\mathrm{ref}}$ is negatively related to PET–ET and positively related to $1/H_c$, with greater sensitivity to PET–ET (-0.198 ± 0.018) than to $1/H_c$ (0.046 ± 0.011), where the sensitivity coefficients were calculated using the variables' z-scores. We note that multiple variable combinations and the corresponding regression coefficients yield similar model accuracies (Table S1). However, both $1/H_c$ and the dryness index are selected in the majority of the top ten models. Across models, the signs of the relationships between both $1/H_c$ and the dryness index to $g_{s,\mathrm{ref}}$ are also consistent. Mean annual temperature and precipitation are also selected in eight out of the ten top models, although $g_{s,\mathrm{ref}}$ is less sensitive to mean climate conditions than to the dryness index. These findings are robust with respect to the alternative approximations and thresholds for deriving $g_{s,\mathrm{ref}}$ described in Section 2.2. Climate dryness and canopy height are still the most informative variables explaining 38% to 45% of $g_{s,\mathrm{ref}}$ variation, in contrast to 13% to 16% using PFT averages (Fig. S4–S7).

Our results indicate that accounting for climate dryness and canopy height explains more than two times the $g_{s,\mathrm{ref}}$ variation explained by PFT alone. This suggests that a simple and tractable equation can enable significantly more accurate $g_{s,\mathrm{ref}}$ assumptions for use in LSMs. Plants in drier climates tend to exhibit lower $g_{s,\mathrm{ref}}$, which provides the

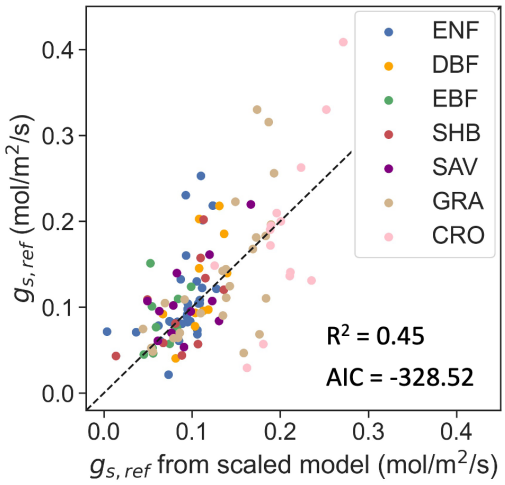

Figure 4. Performance of the best scaled model in estimating $g_{s,\mathrm{ref}}$ using canopy height and climate dryness across sites. Acronyms of PFTs are noted in the caption of Fig. 2.

first ecosystem-scale evidence consistent with leaf scale measurements suggesting species in drier climates tend to have lower stomatal density and area and thus lower unstressed stomatal conductance (Carlson et al., 2016; C. Liu et al., 2018). Based on leaf-level gas exchange, Y.-S. Lin et al. (2015) also found drier climates were correlated with higher marginal water use efficiency, indicating low stomatal conductance under unstressed conditions.

To our knowledge, our study is the first to present evidence on the coordination between unstressed stomatal and xylem conductances (evidenced here through canopy height) at the ecosystem scale. Previous studies have found strong coordination between xylem and stomatal vulnerabilities to water stresses (Martin-StPaul et al., 2017; Brodribb et al., 2017; Pivovaroff et al., 2018), and identified positive $1/H_c$ - $g_{s,\mathrm{ref}}$ relationships based on tree-scale measurements for each species (Schäfer et al., 2000; Ryan et al., 2000; Phillips et al., 2003; Delzon et al., 2004). Our study extends these results by showing that, even without distinguishing species within a PFT, canopy height explains $g_{s,\mathrm{ref}}$ variations at the ecosystem-scale. It further suggests that the direct effect of canopy height on xylem conductance (which suggests a positive relationship between $1/H_c$ and $g_{s,\mathrm{ref}}$) outweighs the influence of xylem conductance's dependence on the sapwood-to-leaf area (which by itself suggests a negative relationship between $1/H_c$ and $g_{s,\mathrm{ref}}$). Nev-

ertheless, these competing influences may explain why, at stand-scale, $g_{s,\mathrm{ref}}$ is less sensitive to canopy height than to climate dryness.

4 Conclusions and implications

This study investigated the spatial variation of stomatal conductance under unstressed conditions ($g_{s,\mathrm{ref}}$) derived from FLUXNET sites across the globe. Differences between PFTs only account for a limited fraction of the total spatial variance. This highlights the uncertainties introduced by PFT-based parameterization schemes commonly used in LSMs. In contrast, using PFT, canopy height and climate dryness significantly contribute to explaining the spatial variation of $g_{s,\mathrm{ref}}$, even in the absence of any information about species composition, competition, soil type (which may affect rooting properties), or other factors. Note that the predictive capabilities of this relationship are not obvious *a priori* from the existence of analogous univariate species-scale relationships. The large range of other factors varying at ecosystem-scale could have prevented the existence of a tractable relationship for $g_{s,\mathrm{ref}}$ with climate dryness and canopy height. Indeed, for water use efficiency (WUE) – another stomatal trait – it has been shown that the WUE aridity index relationship is very different between leaf and ecosystem scales (H. Li et al., 2022). Greater $g_{s,\mathrm{ref}}$ is associated with lower canopy height and more mesic climates, which is supported by ecophysiological theory and is qualitatively consistent with previous evidence observed at leaf and tree scales. Our findings suggest that explicitly considering canopy height and climate dryness can contribute to a more accurate description of unstressed stomatal conductance and its ecohydrological consequences in models. Additionally, an increasing number of land models have started to incorporate plant hydraulics and therefore a mechanistic impact of canopy height on the equivalent $g_{s,\mathrm{ref}}$ (Kennedy et al., 2019; Eller et al., 2020; L. Li et al., 2021). The sensitivity of $g_{s,\mathrm{ref}}$ to canopy height estimated here can provide an observation-based diagnostic benchmark for examining such parameterizations. Overall, the fact that climate and ecological state explain $g_{s,\mathrm{ref}}$ highlights the importance of plant-environment interactions and ecological dynamics in shaping community-average traits. Our findings motivate further studies accounting for these impacts to improve prediction of biosphere-atmosphere interactions.

Open Research

All meteorological data and canopy height data were obtained from the FLUXNET2015 dataset (`https://fluxnet.org/data/fluxnet2015-dataset/`). Leaf area index was extracted from the MODIS product (MCD15A3H.006, https://doi.org/10.5067/MODIS/MCD15A3H.006).

Acknowledgments

AGK was funded by the NASA Modeling, Analysis, and Prediction program, grant 80NSSC21K1523, and by NSF DEB-1942133. QZ was supported by the National Natural Science Foundation of China (no. U2243214). KAN acknowledges support from NSF-DEB 1552747. RDK's involvement with the study was supported by the NASA MAP program. The authors acknowledge the FLUXNET network for providing the FLUXNET2015 dataset.

References

Ackerly, D. D., & Cornwell, W. K. (2007). A trait-based approach to community assembly: partitioning of species trait values into within- and among-community components. *Ecol. Lett.*, *10*(2), 135–145.

Alam, M. S., Lamb, D. W., & Warwick, N. W. M. (2021). A canopy transpiration model based on scaling up stomatal conductance and radiation interception as affected by leaf area index. *Water*, *13*(3). doi: 10.3390/w13030252

Anderegg, W. R. L. (2015). Spatial and temporal variation in plant hydraulic traits and their relevance for climate change impacts on vegetation. *New Phytol.*, *205*(3), 1008–1014.

Anderegg, W. R. L., Wolf, A., Arango-Velez, A., Choat, B., Chmura, D. J., Jansen, S., ... Pacala, S. (2018). Woody plants optimise stomatal behaviour relative to hydraulic risk. *Ecol. Lett.*, *21*(7), 968–977.

Ball, J. T., Woodrow, I. E., & Berry, J. A. (1987). A model predicting stomatal conductance and its contribution to the control of photosynthesis under different environmental conditions. In J. Biggins (Ed.), *Progress in photosynthesis research: Volume 4 proceedings of the VIIth international congress on photosynthesis providence, rhode island, USA, august 10–15, 1986* (pp. 221–224). Dordrecht: Springer Netherlands.

Bonan, G., Williams, M., Fisher, R., & Oleson, K. (2014). Modeling stomatal conductance in the earth system: linking leaf water-use efficiency and water

transport along the soil–plant–atmosphere continuum. *Geoscientific Model Development*, *7*(5), 2193–2222.

Brodribb, T. J., & Jordan, G. J. (2011). Water supply and demand remain balanced during leaf acclimation of nothofagus cunninghamii trees. *New Phytologist*, *192*(2), 437–448.

Brodribb, T. J., McAdam, S. A., & Carins Murphy, M. R. (2017). Xylem and stomata, coordinated through time and space. *Plant, Cell & Environment*, *40*(6), 872–880.

Buckley, T. N., & Mott, K. A. (2013). Modelling stomatal conductance in response to environmental factors. *Plant, cell & environment*, *36*(9), 1691–1699.

Carlson, J. E., Adams, C. A., & Holsinger, K. E. (2016). Intraspecific variation in stomatal traits, leaf traits and physiology reflects adaptation along aridity gradients in a south african shrub. *Ann. Bot.*, *117*(1), 195–207.

Cornwell, W. K., Schwilk, L. D. W., & Ackerly, D. D. (2006). A trait-based test for habitat filtering: convex hull volume. *Ecology*, *87*(6), 1465–1471.

Delzon, S., Sartore, M., Burlett, R., Dewar, R., & Loustau, D. (2004). Hydraulic responses to height growth in maritime pine trees. *Plant, Cell & Environment*, *27*(9), 1077–1087.

Dow, G. J., Bergmann, D. C., & Berry, J. A. (2014). An integrated model of stomatal development and leaf physiology. *New Phytologist*, *201*(4), 1218–1226.

Duursma, R. A., Blackman, C. J., Lopéz, R., Martin-StPaul, N. K., Cochard, H., & Medlyn, B. E. (2019). On the minimum leaf conductance: its role in models of plant water use, and ecological and environmental controls. *New Phytologist*, *221*(2), 693–705.

Efron, B. (1992). Bootstrap methods: another look at the jackknife. In *Breakthroughs in statistics* (pp. 569–593). Springer.

Eller, C. B., Rowland, L., Mencuccini, M., Rosas, T., Williams, K., Harper, A., ... others (2020). Stomatal optimization based on xylem hydraulics (sox) improves land surface model simulation of vegetation responses to climate. *New Phytologist*, *226*(6), 1622–1637.

Fischer, D. G., Kolb, T. E., & DeWald, L. E. (2002). Changes in whole-tree water relations during ontogeny of pinus flexilis and pinus ponderosa in a high-elevation meadow. *Tree Physiology*, *22*(10), 675–685.

FLUXNET. (2016). *FLUXNET 2015 tier 1 dataset.* (Available at `http://fluxnet.fluxdata.org/data/fluxnet2015-dataset/`. Accessed July 25, 2018)

Fowler, M. D., Kooperman, G. J., Randerson, J. T., & Pritchard, M. S. (2019). The effect of plant physiological responses to rising co 2 on global streamflow. *Nature Climate Change*, *9*(11), 873–879.

Franks, P. J., Bonan, G. B., Berry, J. A., Lombardozzi, D. L., Holbrook, N. M., Herold, N., & Oleson, K. W. (2018). Comparing optimal and empirical stomatal conductance models for application in earth system models. *Glob. Chang. Biol.*, *24*(12), 5708–5723.

Franks, P. J., Drake, P. L., & Beerling, D. J. (2009). Plasticity in maximum stomatal conductance constrained by negative correlation between stomatal size and density: an analysis using eucalyptus globulus. *Plant, cell & environment*, *32*(12), 1737–1748.

Garcia, E. S., Swann, A. L. S., Villegas, J. C., Breshears, D. D., Law, D. J., Saleska, S. R., & Stark, S. C. (2016). Synergistic ecoclimate teleconnections from forest loss in different regions structure global ecological responses. *PLoS One*, *11*(11), e0165042.

Granier, A., Loustau, D., & Bréda, N. (2000). A generic model of forest canopy conductance dependent on climate, soil water availability and leaf area index. *Annals of forest science*, *57*(8), 755–765.

Green, J. K., Konings, A. G., Alemohammad, S. H., Berry, J., Entekhabi, D., Kolassa, J., ... Gentine, P. (2017). Regionally strong feedbacks between the atmosphere and terrestrial biosphere. *Nature Geoscience*, *10*(6), 410–414.

Hetherington, A. M., & Woodward, F. I. (2003). The role of stomata in sensing and driving environmental change. *Nature*, *424*(6951), 901–908.

Jarvis, P. (1976). The interpretation of the variations in leaf water potential and stomatal conductance found in canopies in the field. *Philosophical Transactions of the Royal Society of London. B, Biological Sciences*, *273*(927), 593–610.

Kala, J., De Kauwe, M. G., Pitman, A. J., Medlyn, B. E., Wang, Y.-P., Lorenz, R., & Perkins-Kirkpatrick, S. E. (2016). Impact of the representation of stomatal conductance on model projections of heatwave intensity. *Scientific reports*, *6*(1), 1–7.

Kennedy, D., Swenson, S., Oleson, K. W., Lawrence, D. M., Fisher, R., Lola da

Costa, A. C., & Gentine, P. (2019). Implementing plant hydraulics in the community land model, version 5. *Journal of Advances in Modeling Earth Systems*, *11*(2), 485–513.

Koenker, R. (2005). *Quantile regression*. Cambridge University Press. doi: 10.1017/CBO9780511754098

Konings, A. G., & Gentine, P. (2017). Global variations in ecosystem-scale isohydricity. *Global change biology*, *23*(2), 891–905.

Konings, A. G., Williams, A., & Gentine, P. (2017). Sensitivity of grassland productivity to aridity controlled by stomatal and xylem regulation. *Nature Geoscience*, *10*(4), 284–288.

Lammertsma, E. I., de Boer, H. J., Dekker, S. C., Dilcher, D. L., Lotter, A. F., & Wagner-Cremer, F. (2011). Global CO2 rise leads to reduced maximum stomatal conductance in florida vegetation. *Proc. Natl. Acad. Sci. U. S. A.*, *108*(10), 4035–4040.

Lawrence, D. M., Fisher, R. A., Koven, C. D., Oleson, K. W., Swenson, S. C., Bonan, G., ... others (2019). The community land model version 5: Description of new features, benchmarking, and impact of forcing uncertainty. *Journal of Advances in Modeling Earth Systems*, *11*(12), 4245–4287.

Li, H., Wei, M., Dong, L., Hu, W., Xiong, J., Sun, Y., ... others (2022). Leaf and ecosystem water use efficiencies differ in their global-scale patterns and drivers. *Agricultural and Forest Meteorology*, *319*, 108919.

Li, L., Yang, Z.-L., Matheny, A. M., Zheng, H., Swenson, S. C., Lawrence, D. M., ... Leung, L. R. (2021). Representation of plant hydraulics in the noah-mp land surface model: Model development and multiscale evaluation. *Journal of Advances in Modeling Earth Systems*, *13*(4), e2020MS002214.

Li, X., Gentine, P., Lin, C., Zhou, S., Sun, Z., Zheng, Y., ... Zheng, C. (2019). A simple and objective method to partition evapotranspiration into transpiration and evaporation at eddy-covariance sites. *Agricultural and Forest Meteorology*, *265*, 171–182.

Lin, C., Gentine, P., Huang, Y., Guan, K., Kimm, H., & Zhou, S. (2018). Diel ecosystem conductance response to vapor pressure deficit is suboptimal and independent of soil moisture. *Agricultural and Forest Meteorology*, *250*, 24–34.

Lin, Y.-S., Medlyn, B. E., Duursma, R. A., Prentice, I. C., Wang, H., Baig, S., ...

others (2015). Optimal stomatal behaviour around the world. *Nature Climate Change*, *5*(5), 459–464.

Liu, C., He, N., Zhang, J., Li, Y., Wang, Q., Sack, L., & Yu, G. (2018). Variation of stomatal traits from cold temperate to tropical forests and association with water use efficiency. *Funct. Ecol.*, *32*(1), 20–28.

Liu, Y., Holtzman, N. M., & Konings, A. G. (2021). Global ecosystem-scale plant hydraulic traits retrieved using model–data fusion. *Hydrology and Earth System Sciences*, *25*(5), 2399–2417.

Liu, Y., Kumar, M., Katul, G. G., Feng, X., & Konings, A. G. (2020). Plant hydraulics accentuates the effect of atmospheric moisture stress on transpiration. *Nature Climate Change*, *10*(7), 691–695.

Mankin, J. S., Seager, R., Smerdon, J. E., Cook, B. I., & Williams, A. P. (2019). Mid-latitude freshwater availability reduced by projected vegetation responses to climate change. *Nature Geoscience*, *12*(12), 983–988.

Manzoni, S., Vico, G., Porporato, A., & Katul, G. (2013). Biological constraints on water transport in the soil–plant–atmosphere system. *Advances in Water Resources*, *51*, 292–304.

Martin-StPaul, N., Delzon, S., & Cochard, H. (2017). Plant resistance to drought depends on timely stomatal closure. *Ecology Letters*, *20*(11), 1437–1447.

McDowell, N. G., Barnard, H., Bond, B., Hinckley, T., Hubbard, R., Ishii, H., ... others (2002). The relationship between tree height and leaf area: sapwood area ratio. *Oecologia*, *132*(1), 12–20.

McDowell, N. G., Beerling, D. J., Breshears, D. D., Fisher, R. A., Raffa, K. F., & Stitt, M. (2011). The interdependence of mechanisms underlying climate-driven vegetation mortality. *Trends in ecology & evolution*, *26*(10), 523–532.

McElwain, J. C., Yiotis, C., & Lawson, T. (2016). Using modern plant trait relationships between observed and theoretical maximum stomatal conductance and vein density to examine patterns of plant macroevolution. *New Phytologist*, *209*(1), 94–103.

Medlyn, B. E., Duursma, R. A., Eamus, D., Ellsworth, D. S., Prentice, I. C., Barton, C. V. M., ... Wingate, L. (2011). Reconciling the optimal and empirical approaches to modelling stomatal conductance. *Glob. Chang. Biol.*, *17*(6), 2134–2144.

Monteith, J. L. (1965). Evaporation and environment. In *Symposia of the society for experimental biology* (Vol. 19, pp. 205–234).

Myneni, R., Knyazikhin, Y., & Park, T. (2015). *MCD15A3H MODIS/Terra+Aqua Leaf Area Index/FPAR 4-day L4 Global 500m SIN Grid V006.* (NASA EOSDIS Land Processes DAAC. Accessed on 2020-04-27. doi:10.5067/MODIS/MCD15A3H.006)

Novick, K. A., Ficklin, D. L., Stoy, P. C., Williams, C. A., Bohrer, G., Christopher Oishi, A., ... Phillips, R. P. (2016). The increasing importance of atmospheric demand for ecosystem water and carbon fluxes. *Nat. Clim. Chang.*, *6*(11), 1023–1027.

Novick, K. A., Oren, R., Stoy, P., Juang, J.-Y., Siqueira, M., & Katul, G. (2009). The relationship between reference canopy conductance and simplified hydraulic architecture. *Adv. Water Resour.*, *32*(6), 809–819.

Oleson, K. W., Lawrence, D. M., Bonan, G. B., Drewniak, B., Huang, M., Koven, C. D., ... others (2013). *Technical description of version 4.5 of the Community Land Model (CLM)* (Tech. Rep.). National Center for Atmospheric Research, Boulder, Colorado. (NCAR Technical Note NCAR/TN-503+STR)

Oren, R., Sperry, J., Katul, G., Pataki, D., Ewers, B., Phillips, N., & Schäfer, K. (1999). Survey and synthesis of intra-and interspecific variation in stomatal sensitivity to vapour pressure deficit. *Plant, Cell & Environment*, *22*(12), 1515–1526.

Penman, H. L. (1948). Natural evaporation from open water, bare soil and grass. *Proceedings of the Royal Society of London. Series A. Mathematical and Physical Sciences*, *193*(1032), 120–145.

Phillips, N., Bond, B., McDowell, N., Ryan, M. G., & Schauer, A. (2003). Leaf area compounds height-related hydraulic costs of water transport in oregon white oak trees. *Functional Ecology*, *17*(6), 832–840.

Pivovaroff, A. L., Cook, V. M., & Santiago, L. S. (2018). Stomatal behaviour and stem xylem traits are coordinated for woody plant species under exceptional drought conditions. *Plant, cell & environment*, *41*(11), 2617–2626.

Powell, T. L., Galbraith, D. R., Christoffersen, B. O., Harper, A., Imbuzeiro, H. M., Rowland, L., ... others (2013). Confronting model predictions of carbon fluxes with measurements of amazon forests subjected to experimental drought. *New*

Phytologist, *200*(2), 350–365.

Rodell, M., Houser, P., Jambor, U., Gottschalck, J., Mitchell, K., Meng, C.-J., ... others (2004). The global land data assimilation system. *Bulletin of the American Meteorological Society*, *85*(3), 381–394.

Ryan, M. G., Bond, B. J., Law, B. E., Hubbard, R. M., Woodruff, D., Cienciala, E., & Kucera, J. (2000). Transpiration and whole-tree conductance in ponderosa pine trees of different heights. *Oecologia*, *124*(4), 553–560.

Ryan, M. G., Phillips, N., & Bond, B. J. (2006). The hydraulic limitation hypothesis revisited. *Plant, Cell & Environment*, *29*(3), 367–381.

Schäfer, K., Oren, R., & Tenhunen, J. (2000). The effect of tree height on crown level stomatal conductance. *Plant, Cell & Environment*, *23*(4), 365–375.

Sperry, J. S., Venturas, M. D., Anderegg, W. R., Mencuccini, M., Mackay, D. S., Wang, Y., & Love, D. M. (2017). Predicting stomatal responses to the environment from the optimization of photosynthetic gain and hydraulic cost. *Plant, cell & environment*, *40*(6), 816–830.

Stark, S. C., Breshears, D. D., Garcia, E. S., Law, D. J., Minor, D. M., Saleska, S. R., ... Redmond, M. D. (2016). Toward accounting for ecoclimate teleconnections: intra- and inter-continental consequences of altered energy balance after vegetation change. *Landsc. Ecol.*, *31*(1), 181–194.

Trugman, A. T., Medvigy, D., Mankin, J. S., & Anderegg, W. R. L. (2018). Soil moisture stress as a major driver of carbon cycle uncertainty. *Geophys. Res. Lett.*, *45*(13), 6495–6503.

Tyree, M. T., & Ewers, F. W. (1991). The hydraulic architecture of trees and other woody plants. *New Phytologist*, *119*(3), 345–360.

Verheijen, L. M., Aerts, R., Brovkin, V., Cavender-Bares, J., Cornelissen, J. H. C., Kattge, J., & van Bodegom, P. M. (2015). Inclusion of ecologically based trait variation in plant functional types reduces the projected land carbon sink in an earth system model. *Glob. Chang. Biol.*, *21*(8), 3074–3086.

Walker, A. P., Quaife, T., van Bodegom, P. M., De Kauwe, M. G., Keenan, T. F., Joiner, J., ... Woodward, F. I. (2017). The impact of alternative trait-scaling hypotheses for the maximum photosynthetic carboxylation rate (vcmax) on global gross primary production. *New Phytol.*, *215*(4), 1370–1386.

Wehr, R., & Saleska, S. R. (2021). Calculating canopy stomatal conductance from

eddy covariance measurements, in light of the energy budget closure problem. *Biogeosciences*, *18*(1), 13–24.

Wolz, K. J., Wertin, T. M., Abordo, M., Wang, D., & Leakey, A. D. (2017). Diversity in stomatal function is integral to modelling plant carbon and water fluxes. *Nature Ecology & Evolution*, *1*(9), 1292–1298.

Wu, G., Hu, Z., Keenan, T. F., Li, S., Zhao, W., Cao, R. C., ... Sun, X. (2020). Incorporating spatial variations in parameters for improvements of an evapotranspiration model. *Journal of Geophysical Research: Biogeosciences*, *125*(11), e2019JG005504.

Zhang, Q., Ficklin, D. L., Manzoni, S., Wang, L., Way, D., Phillips, R. P., & Novick, K. A. (2019). Response of ecosystem intrinsic water use efficiency and gross primary productivity to rising vapor pressure deficit. *Environ. Res. Lett.*, *14*(7), 074023.

Figure 1.

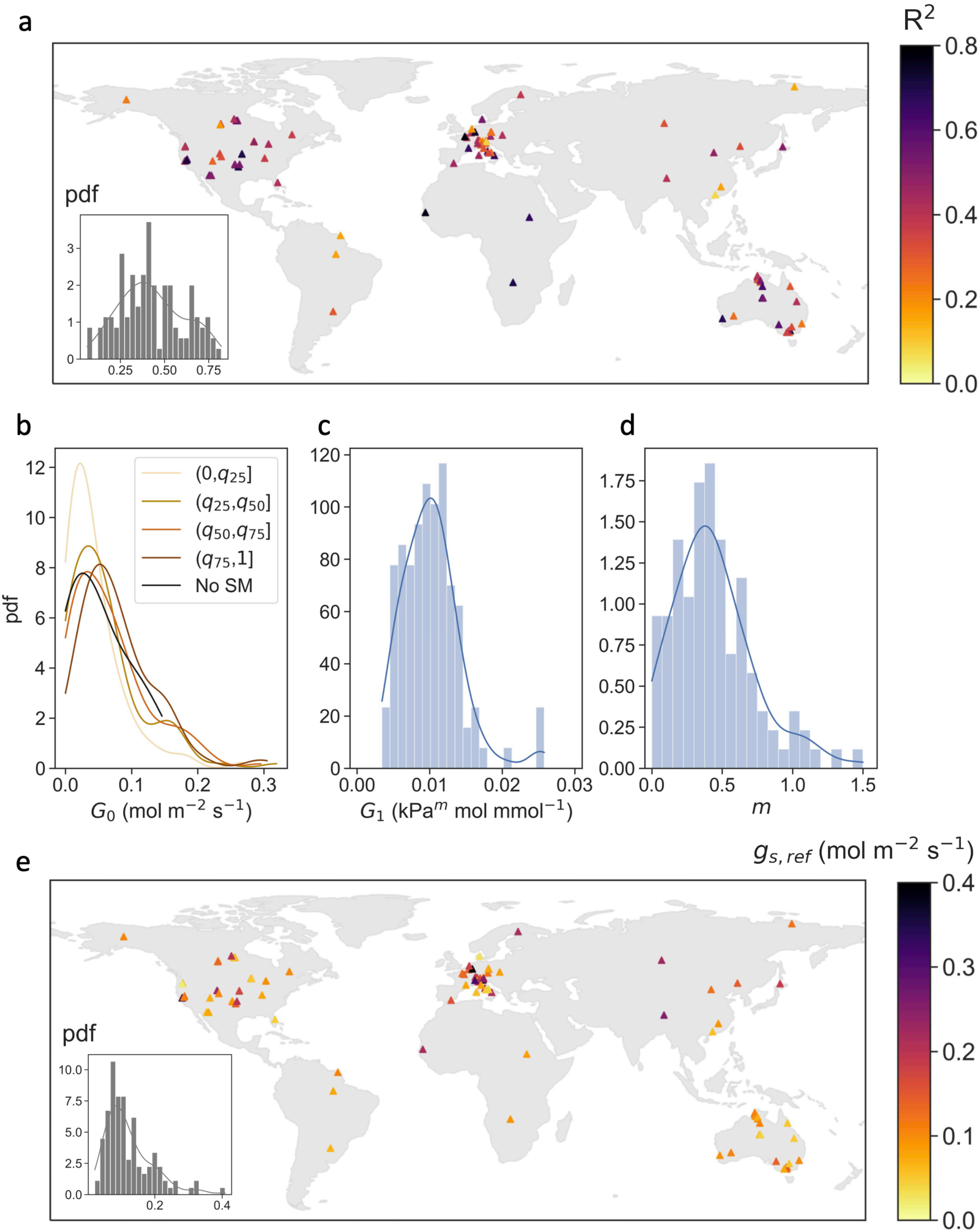
a
R2
0.8
0.6
0.4
0.2
0.0
pdf
3
2
1
0
0.25
0.50
0.75
b
12
10
8
6
4
2
0
pdf
(0,q25]
(q25,q50]
(q50,q75]
(q75,1]
No SM
0.0
0.1
0.2
0.3
G0 (mol m−2 s−1)
c
120
100
80
60
40
20
0
0.00
0.01
0.02
0.03
G1 (kPam mol mmol−1)
d
1.75
1.50
1.25
1.00
0.75
0.50
0.25
0.00
0.0
0.5
1.0
1.5
m
e
gs, ref (mol m−2 s−1)
0.4
0.3
0.2
0.1
0.0
pdf
10.0
7.5
5.0
2.5
0.0
0.2
0.4

Figure 2.

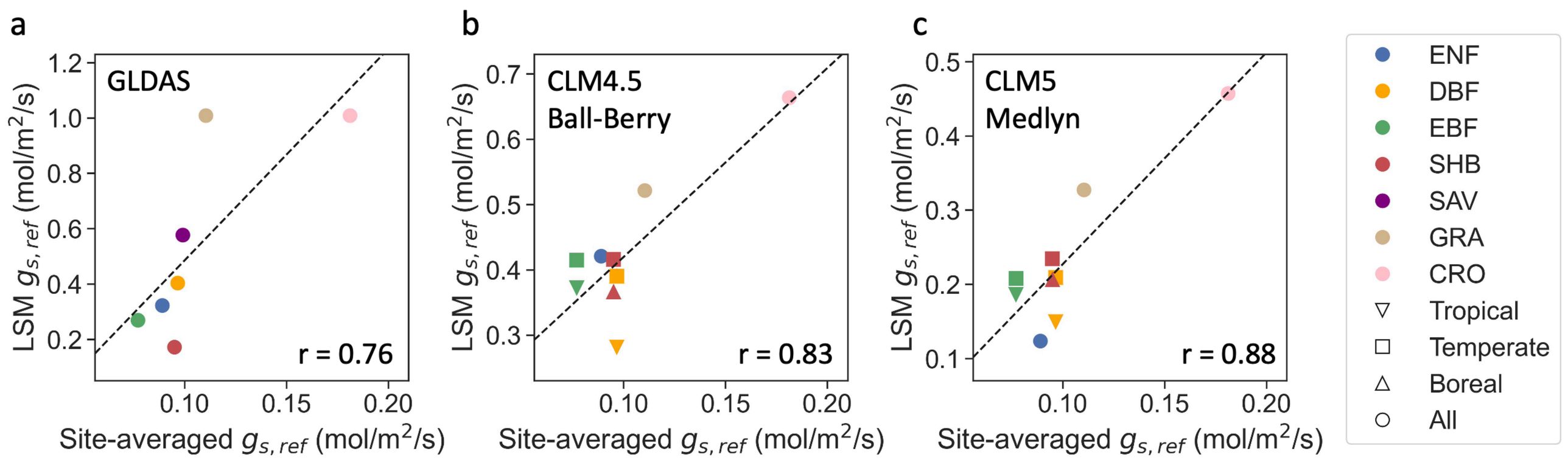
a
GLDAS
r = 0.76
LSM $g_{s,ref}$ (mol/m^2/s)
Site-averaged $g_{s,ref}$ (mol/m^2/s)
b
CLM4.5
Ball-Berry
r = 0.83
LSM $g_{s,ref}$ (mol/m^2/s)
Site-averaged $g_{s,ref}$ (mol/m^2/s)
c
CLM5
Medlyn
r = 0.88
LSM $g_{s,ref}$ (mol/m^2/s)
Site-averaged $g_{s,ref}$ (mol/m^2/s)
ENF
DBF
EBF
SHB
SAV
GRA
CRO
Tropical
Temperate
Boreal
All

Figure 3.

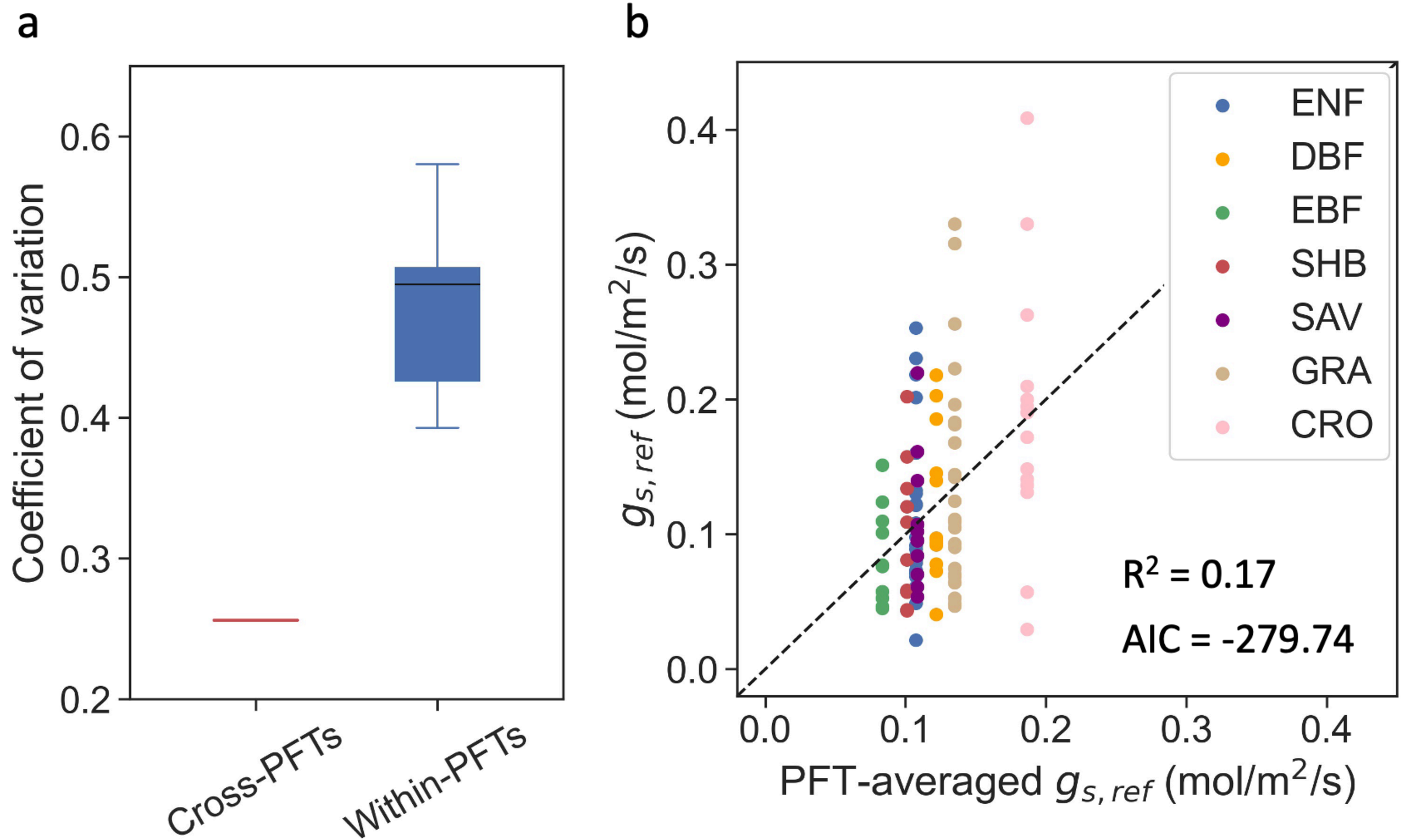
a
b
Coefficient of variation
0.6
0.5
0.4
0.3
0.2
Cross-PFTs
Within-PFTs
$g_{s,\,ref}$ (mol/m^2/s)
0.4
0.3
0.2
0.1
0.0
ENF
DBF
EBF
SHB
SAV
GRA
CRO
R^2 = 0.17
AIC = -279.74
0.0
0.1
0.2
0.3
0.4
PFT-averaged $g_{s,\,ref}$ (mol/m^2/s)

Figure 4.

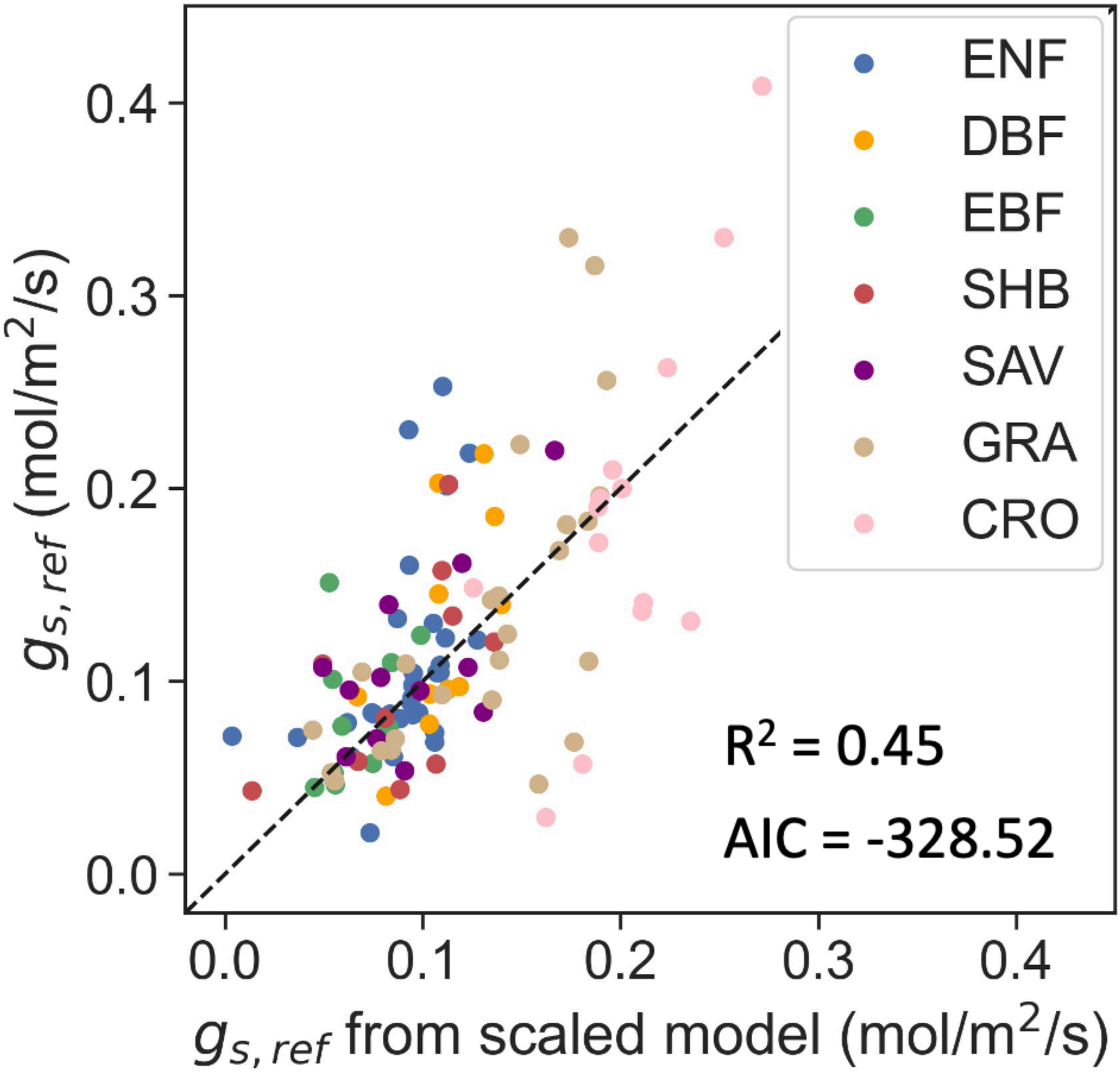
ENF
DBF
EBF
SHB
SAV
GRA
CRO
R^2 = 0.45
AIC = -328.52
0.0
0.1
0.2
0.3
0.4
$g_{s,ref}$ (mol/m^2/s)
$g_{s,ref}$ from scaled model (mol/m^2/s)

Supporting Information for "Canopy height and climate dryness parsimoniously explain spatial variations of unstressed stomatal conductance"

Yanlan Liu [1,2], Olivia Flournoy [3], Quan Zhang [4], Kimberly A. Novick [5],

Randal D. Koster [6], Alexandra G. Konings [7]

[1]School of Earth Sciences, The Ohio State University, Columbus, OH, USA

[2]School of Environment and Natural Resources, The Ohio State University, Columbus, OH, USA

[3]Department of Geophysics, Stanford University, Stanford, CA, USA

[4]State Key Laboratory of Water Resources and Hydropower Engineering Science, Wuhan University, Wuhan, China

[5]O'Neill School of Public and Environmental Affairs, Indiana University Bloomington, Bloomington, IN, USA

[6]Global Modeling and Assimilation Office, NASA GSFC, Greenbelt, MD, USA

[7]Department of Earth System Science, Stanford University, Stanford, CA, USA

Contents of this file

Table S1. Accuracies and selected variables of the top ten scaled models based on AIC. The coefficients in front of the selected variables are the regression coefficients (β in Eq. 4 of the main text) of the normalized variables (z-scores), representing the sensitivities of $g_{s,\mathrm{ref}}$ to the selected variables. $g_{s,\mathrm{ref}}$ of each site is the 90th percentile of stomatal conductance derived using $g_s = (G_s - G_0)/\min(\mathrm{LAI}, 6)$.

			Selected variables		
Model	R^2	AIC	Canopy height	Dryness index	Mean climate
1	0.45	−328.52	$+0.046/H_c$	−0.198(PET − ET)	
2	0.44	−328.50		−0.201(PET − ET)	
3	0.44	−326.72		−0.212(PET − ET)	−0.016MAP
4	0.45	−326.63	$+0.047/H_c$	−0.208(PET − ET)	−0.007MAT
5	0.43	−326.62		−0.229(PET − ET)	+0.026MAT
6	0.45	−326.47	$+0.043/H_c$	−0.209(PET − ET)	−0.015MAP
7	0.40	−320.53		−0.155PET/ET	−0.071MAT
8	0.41	−319.56	$+0.063/H_c$	−0.139PET/ET	−0.053MAT
9	0.39	−316.12		−0.155PET/ET	−0.039MAP
10	0.40	−315.69	$+0.051/H_c$	−0.149PET/ET	−0.030MAP

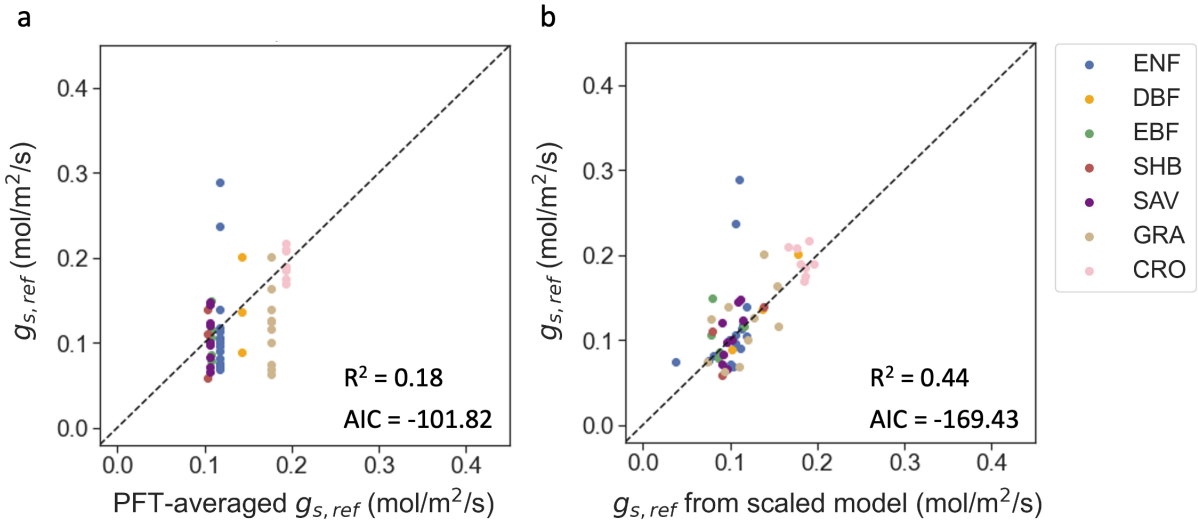

Figure S1. Comparison between gs,ref derived from observations (y-axis) and those estimated using (a) the baseline model (PFT-averages) and (b) the best scaled model, color coded by PFTs. Here, gs,ref is derived as described in the main text, but using only data when the energy closure error is below a threshold of 18%, which is the average across time and sites. The energy closure error is calculated as the difference between net radiation and the summation of latent, sensible, and ground heat fluxes, normalized by the net radiation. Only sites with available downward and upward longwave and shortwave radiation and ground heat flux observations and with at least 100 observations satisfying all quality-control filters are analyzed. The $\beta^T X$ in Eq. (4) of the best scaled model is $0.64 - 0.108\,(\mathrm{PET} - \mathrm{ET}) - 0.062\,\mathrm{MAT}$, followed by $0.63 + 0.050/H_c - 0.088\,(\mathrm{PET} - \mathrm{ET}) - 0.057\,\mathrm{MAT}$, where $1/H_c$, $\mathrm{PET} - \mathrm{ET}$, and MAT are z-scores of the corresponding variables.

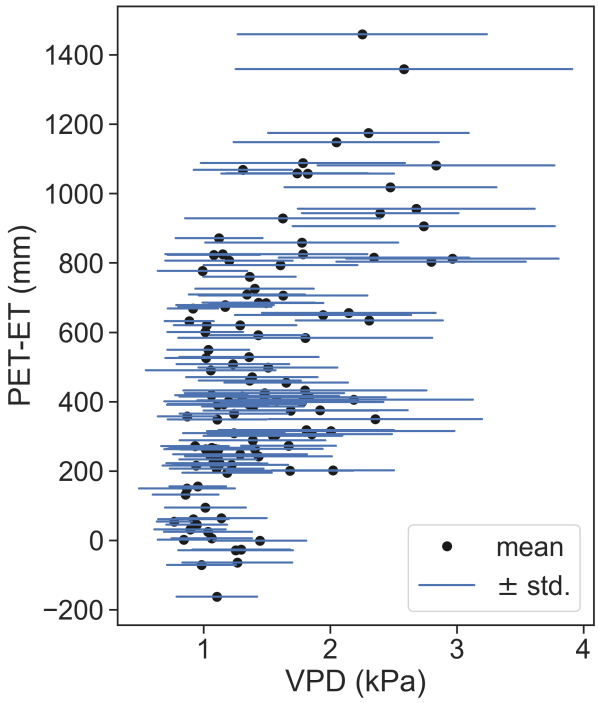

Figure S2. Relation between dryness index (long-term averaged annual PET-ET) and vapor pressure deficit (VPD) when the stomatal conductance g_s is close to $g_{s,\mathrm{ref}}$, i.e., within the range of 85th and 95th percentiles. Each black dot shows the mean and each horizontal blue line shows the standard deviation of VPD when g_s is close to $g_{s,\mathrm{ref}}$ at each site.

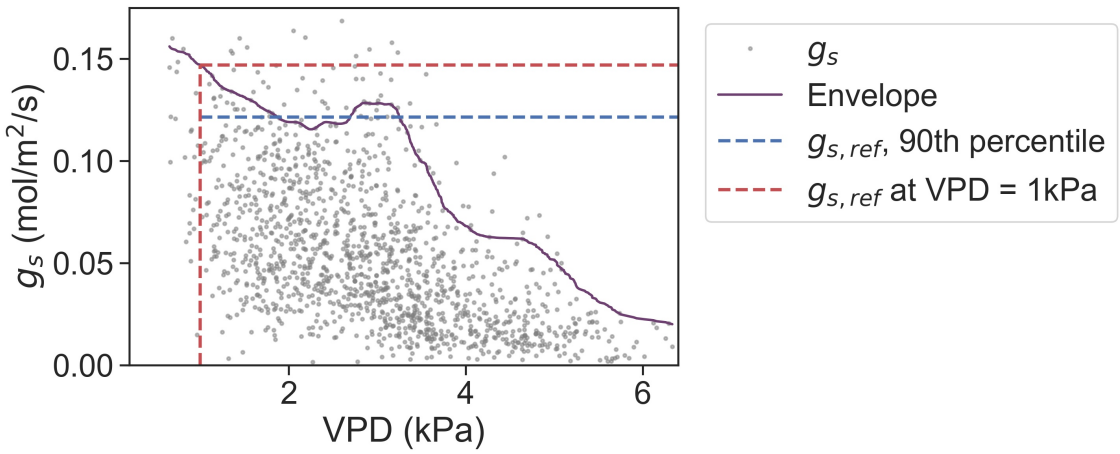

Figure S3. An example of deriving unstressed stomatal conductance ($g_{s,\mathrm{ref}}$) as the 90th percentile of stomatal conductance (g_s) at all times and as the envelope at VPD of 1 kPa, respectively, at the AR-Vir site. Grey dots are g_s derived from half-hourly observations satisfying the filters (described in Section 2.2.) across the entire record. The purple line shows the upper envelope of g_s, calculated using a quantile regression (Koenker, 2005) that estimates the 90th quantile of g_s in response to VPD using the *cvxpy* software in Python. The blue and red dashed lines denote the 90th percentile of g_s and the envelope at VPD of 1kPa, respectively.

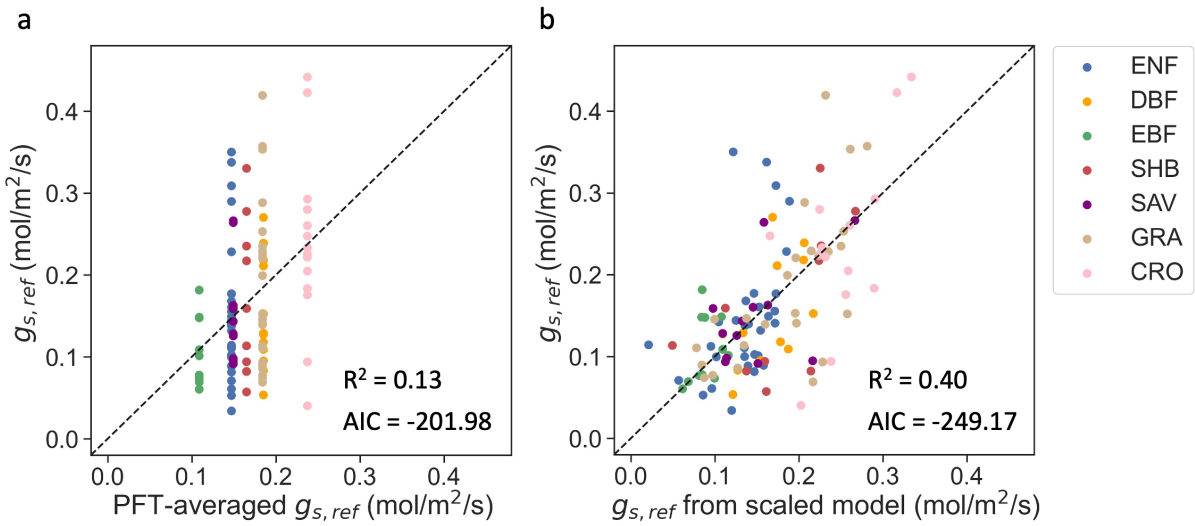

Figure S4. Comparison between $g_{s,\mathrm{ref}}$ derived from observations (y-axis) and those estimated using (a) the baseline model (PFT-averages) and (b) the best scaled model, color coded by PFTs. Here, $g_{s,\mathrm{ref}}$ is the 90th percentile of stomatal conductance (g_s) at all times, which was derived assuming ecosystem conductance G_s represents canopy conductance, i.e., replacing Eq. (2) in the main text with $g_s = G_s/\min(\mathrm{LAI}, 6)$. The $\beta^T X$ in Eq. (4) of the best scaled model is $0.76 + 0.075/H_c - 0.221(\mathrm{PET} - \mathrm{ET}) - 0.053\mathrm{MAP}$, where $1/H_c$, $\mathrm{PET} - \mathrm{ET}$, and MAP are z-scores of the corresponding variables.

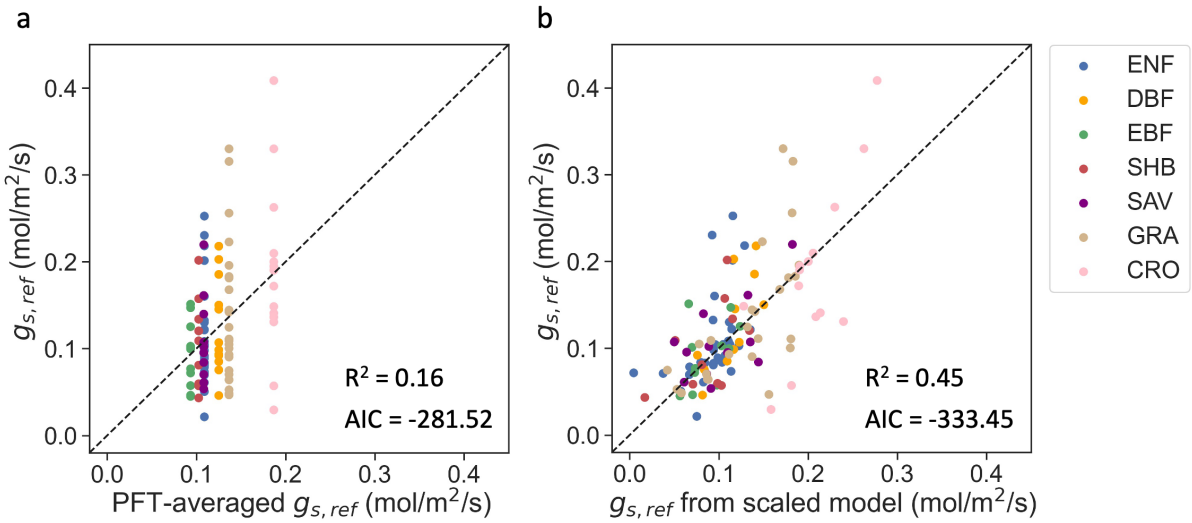

Figure S5. Comparison between $g_{s,\mathrm{ref}}$ derived from observations (y-axis) and those estimated using (a) the baseline model (PFT-averages) and (b) the best scaled model, color coded by PFTs. Here, $g_{s,\mathrm{ref}}$ is the 90th percentile of stomatal conductance (g_s) at all times, which was derived using a LAI cut-off of 4, i.e., $g_s = (G_s - G_0)/\min(\mathrm{LAI}, 4)$. The $\beta^T X$ in Eq. (4) of the best scaled model is $0.66 + 0.038/H_c - 0.223(\mathrm{PET} - \mathrm{ET}) + 0.036\mathrm{MAT}$, where $1/H_c$, $\mathrm{PET} - \mathrm{ET}$, and MAT are z-scores of the corresponding variables.

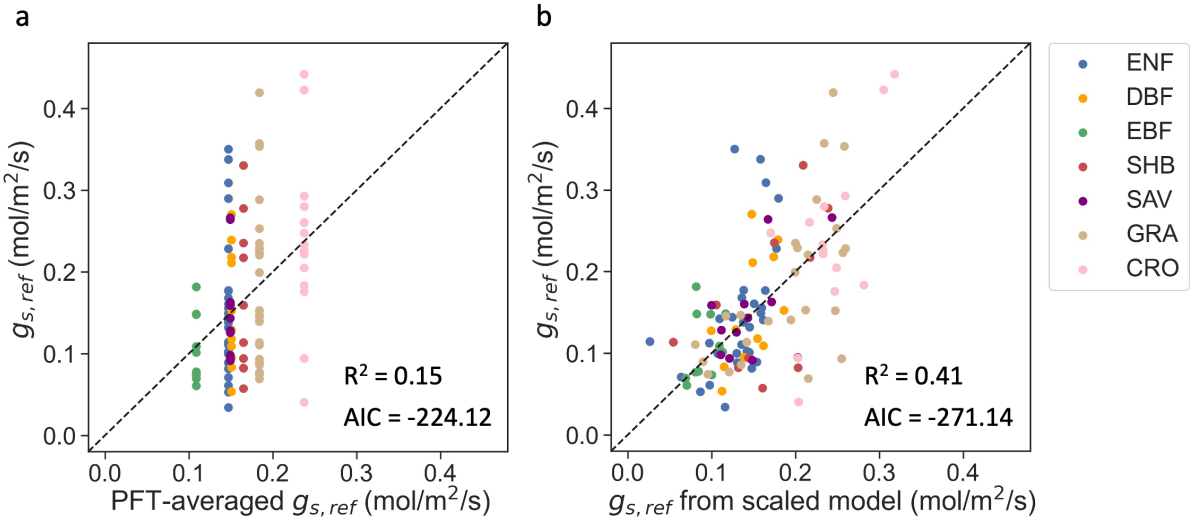

Figure S6. Same as Fig. S4 except that a LAI cut-off of 8 was used, i.e., $g_s = (G_s - G_0)/\min(\mathrm{LAI}, 8)$. The $\beta^T X$ in Eq. (4) of the best scaled model is $0.81 - 0.230(\mathrm{PET} - \mathrm{ET}) - 0.033\mathrm{MAP}$. The $\beta^T X$ of the second best (AIC = -270.93, $\mathrm{R}^2 = 0.42$) scaled model is $0.75 + 0.077/H_c - 0.213(\mathrm{PET} - \mathrm{ET}) - 0.028\mathrm{MAP}$, where $1/H_c$, $\mathrm{PET} - \mathrm{ET}$, and MAP are z-scores of the corresponding variables.

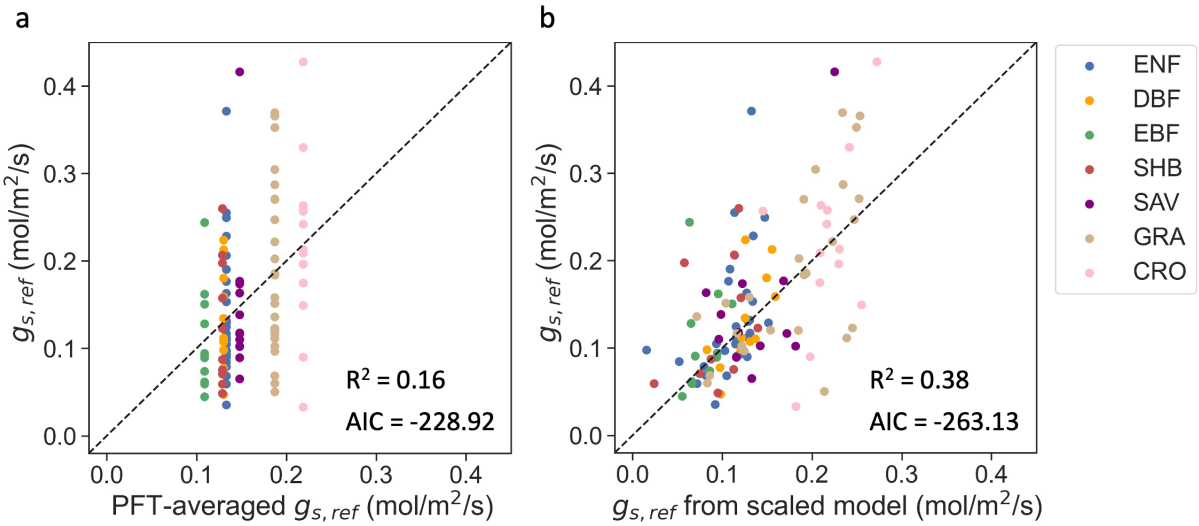

Figure S7. Comparison between $g_{s,\mathrm{ref}}$ derived from observations (y-axis) and those estimated using (a) the baseline model (PFT-averages) and (b) the best scaled model, color coded by PFTs. Here, $g_{s,\mathrm{ref}}$ is the envelope of stomatal conductance when VPD = 1 kPa, estimated using quantile regression as illustrated in Fig. S2. The stomatal conductance was derived using Eq.(2) in the main text. The $\beta^T X$ in Eq. (4) of the best scaled model is $0.71 + 0.041/H_c - 0.197(\mathrm{PET} - \mathrm{ET})$, where $1/H_c$ and $\mathrm{PET} - \mathrm{ET}$ are z-scores of the corresponding variables.